Article Title: **MC1R drives cutaneous repair by promoting wound angiogenesis and lymphangiogenesis**

Running title: MC1R drives cutaneous wound repair

AUTHORS:

Holly Rocliffe[1], Shani Austin-Williams[2*], Georgios Krilis[3*], Kanheng Zhou[4], Yubo Ji[4], Connor Bain[5], Yonlada Nawilaijaroen[1], Antonella Pellicoro[1], Tianchi Zhou[1], Michael Crichton[5], Zhihong Huang[4], Andrea Caporali[3], Jenna L Cash[1#]

1. Centre for Inflammation Research, Institute for Regeneration and Repair, 47 Little France Crescent, University of Edinburgh, Edinburgh, EH16 4TJ.
2. Biochemical Pharmacology, William Harvey Research Institute, Barts and the London School of Medicine and Dentistry, Charterhouse Square, London, EC1M 6BQ, UK.
3. Centre for Cardiovascular Research, The Queen's Medical Research Institute, 47 Little France Crescent, University of Edinburgh, Edinburgh, EH16 4TJ.
4. School of Science and Engineering, Fulton Building, University of Dundee, Dundee, DD1 4HN, UK
5. Institute of Mechanical, Process and Energy Engineering, School of Engineering and Physical Sciences, Heriot-Watt University, Edinburgh, EH14 4AS, UK

* Equally contributed

CORRESPONDING AUTHOR:

Jenna L Cash

Centre for Inflammation Research

The Queen's Medical Research Institute

47 Little France Crescent

University of Edinburgh

Edinburgh, EH16 4TJ

UK

Jenna.cash@ed.ac.uk

Tel: +44 (0)131 242 6655

MC1R drives cutaneous repair by promoting angiogenesis and lymphangiogenesis

Abstract

Cutaneous wound healing typically results in scarring; however, chronic wounds (CWs) represent a global and escalating health burden causing substantial morbidity and mortality. Estimated to cost Medicare up to $96.8 billion pa and with a profound paucity of effective therapeutics, novel interventions to improve healing are urgently needed. In this study, we assess the impact of manipulating the melanocortin 1 receptor (MC1R) on acute wound healing using a selective agonist, BMS-470539 (MC1R-Ag). MC1R agonism resulted in accelerated wound closure and reepithelialisation in wildtype but not MC1Re/e mice, which harbour a non-functional receptor. MC1R-Ag improved wound perfusion and lymphatic drainage by promoting angiogenesis and lymphangiogenesis, reducing local oxidative stress and inflammation with a knock-on effect of reduced scarring. To assess whether manipulating MC1R would be of benefit in pathological healing, we developed a novel murine model of chronic cutaneous wounds. By combining advanced age and locally elevated oxidative stress, factors shown to be present in most human CWs regardless of their category, resultant wounds expand 5-fold into the surrounding tissue, produce exudate and generate slough. Histological comparisons to human CWs demonstrate robust recapitulation of the hallmarks of human disease, including hyperproliferative epidermis, fibrinous exudate and vasculitis. Crucially, our model facilitates the *in vivo* study of candidate therapies to rescue derailed healing responses. We have identified that abrogation of MC1R signalling, using MC1Re/e mice, exacerbates CWs with enhanced exudate and NETosis. In contrast, topical administration of an MC1R agonist following ulcer debridement rescues the healing response, highlighting MC1R agonism as a candidate therapeutic approach for human CWs. We anticipate that our unique model will become a valuable tool to elucidate mechanisms of ulcer development and persistence.

INTRODUCTION

Skin is a fascinating and complex barrier organ comprising multiple layers and cell types that are functionally distinct. Repair of adult cutaneous wounds is typically described in terms of four overlapping, sequential phases: coagulation, inflammation, proliferation/migration and remodelling, culminating in scar formation. Whist most wounds progress through these healing phases uneventfully, with the magnitude of the inflammatory response linked to the extent of the resultant scar, a growing number fail to heal, resulting in a persistent open skin ulcer *(1, 2)*. These chronic wounds (CWs), including venous leg ulcers (VLU), diabetic foot ulcers (DFU) and pressure ulcers (PU), become 'stuck' in a chronically inflamed state, unable to heal effectively. CWs represent a global and escalating health burden due to a sharp rise in worldwide incidence of key comorbidities, including diabetes, obesity and advanced age. CW complications include infection, amputation, sepsis and death; hence they impose substantial morbidity and mortality on the individual, healthcare systems and society, with approximately £12 billion pa spent by the NHS on 3.8 million wounds *(3–5)*.

Whilst many other fields have made inspiring leaps in understanding their respective pathologies resulting the development of promising therapeutics, research into chronic wounds has long been neglected. Firstly, access to human wound biopsies is not trivial since the necessary infrastructure to obtain these is not readily available to many researchers. Secondly, the lack of a humane animal model that faithfully recapitulates the key features of human CWs has severely hampered CW research. These issues have therefore compromised innovation in new therapies, clinical practices and biomarkers *(6–9)*.

To remove a major barrier for chronic wound research, we have developed an ethical, reproducible, genetically tractable model that reproduces key features of human CWs, including hyperproliferative epidermis, parakeratosis, spongiosis, vasculitis, fibrinous exudate, erythrocyte extravasation, wound expansion and slough generation. We specifically sought to develop a model that is broadly relevant across the ulcer categories of VLU, DFU and PU, rather than specifically modelling a certain category. Whilst each type of chronic wound is associated with certain comorbidities, for example PU with conditions causing immobility; at their core they share key features. The overwhelming majority of skin ulcers develop in the over 50s, with 95 percent occurring in the over 60s. In addition, VLU, DFU and PU have been shown to exhibit high levels of wound bed oxidative stress. *(3, 5, 10)*. We therefore used aged animals (18 months) and local elevation of oxidative stress to develop our preclinical model.

This novel model enables the *in vivo* study of candidate therapies to rescue derailed healing responses. Herein, we explore the therapeutic potential of Melanocortin 1 receptor (MC1R) as a novel driver of wound healing. MC1R is a GPCR expressed peripherally in melanocytes and

immune cells, with roles in pigmentation and regulation of anti-oxidative stress mechanisms following UV exposure *(11)*. With a functional MC1R, eumelanin, a black pigment, is preferentially produced. A highly polymorphic gene, *MC1R* loss-of-function SNPs result in preferential production of the yellow-orange pigment, phaeomelanin. The eumelanin-to-phaeomelanin ratio determines skin and hair colour in humans and coat colour in other mammals. A connection between MC1R and the red-hair phenotype was first established in 1995, by Valverde et al. Since then, variants of MC1R have been linked to an increased risk for skin cancer, UV damage, photoaging and more recently with increased severity of post-burn hypertrophic scarring *(12, 13)*. Several studies have explored the role of the receptor in inflammatory responses, including animal models of arthritis. These works have demonstrated that delivery of an MC1R agonist can dampen immune cell recruitment and/or activation and thus inflammation, which in the case of the arthritic joint can prevent cartilage degradation *(14, 15)*. To date, no studies have explored the role of MC1R in acute and chronic skin wounds, however, Muffley *et al* have described dynamic spatial localisation of MC1R during cutaneous wound repair, including expression by keratinocytes and immune cells in the acute wound bed *(11)*. Here, we identify MC1R as a therapeutic target to drive skin repair by promoting wound angiogenesis and lymphangiogenesis.

RESULTS

MC1R accelerates wound healing with reduced scarring

In agreement with Muffley *et all, e*xpression of *mc1r* and endogenous ligand precursor *pomc* was induced in acute wounds, peaking at 1 day post-injury (dpi) and declining to healthy skin levels by 7 dpi in both young (8 w old) and aged (18 m old) mice (Fig.1A). To investigate the role of MC1R in cutaneous wound repair we used a MC1R selective agonist, BMS-470539 (MC1R-Ag) as the endogenous agonist αMSH is also a ligand for MC3R and MC5R. MC1R-Ag or vehicle control were administered topically to 4mm full-thickness excisional wounds immediately after injury (Fig. 1A). Macroscopic analysis revealed accelerated wound closure in MC1R-Ag-treated wounds, with maximum differences at 3 and 7 dpi (Fig.1B, C). Key repair parameters were assessed, including epithelial tongue length and scab presence as measures of reepithelialisation. An epidermal tongue is the portion of epidermis that has proliferated and migrated under the scab and was found to be significantly longer at 3 dpi with MC1R-Ag-treatment (Fig.1D). Using optical coherence tomography (OCT) imaging of the dynamic changes in epidermal thickness during wound healing, we demonstrate that harnessing MC1R results in earlier proliferation of wound edge epidermis (peak at 3 dpi vs 5 dpi with vehicle-treatment; Fig. 1E), this was followed by a quicker reduction in epidermal thickness by 7 dpi (Fig. 1E, F). Since re-epithelialisation was completed earlier in MC1R-Ag-

treated wounds, this resulted in reduced scab presence at 7 dpi (MC1R-Ag, 17.9% of wounds; vehicle, 71.4%; Fig. 1G,H). To determine whether MC1R-Ag improves wound reepithelialisation by directly modulating migration and/or proliferation of epidermal keratinocytes, we made scratch wounds to keratinocyte (HaCaT) monolayers *in vitro*, finding that MC1R-Ag significantly enhanced scratch wound closure over 24 hours (Fig. S1A-C).

Collagen is a major structural component of normal skin and exhibits a basketweave appearance in the dermis, in contrast to scars, which predominantly consist of linear bundles of collagen fibers. To quantify scarring we measured collagen fiber orientation using a novel algorithm (Fig.S2). Unwounded skin exhibited abundant collagen with largely randomly-oriented fibers corresponding with a low alignment index (0.152 ± 0.024 ; Fig. 1I-K). In vehicle-treated day 7 wounds, collagen was laid down in a more linear fashion resulting in a high alignment of 0.58 ± 0.045. Wound treatment with MC1R-Ag, however, resulted in collagen deposition with a more random orientation closer to unwounded dermal collagen organisation, which equated to reduced alignment in comparison to vehicle-treated wounds (0.39 ± 0.036 MC1R-Ag vs 0.58 ± 0.045 vehicle; Fig. 1I-K). We also assessed collagen quantity in Picrosirius Red-stained wound sections, finding that treatment with MC1R-Ag accelerated the rate of collagen deposition (66.9 ± 1.85% MC1R-Ag vs 56.5.2 ± 3.64% vehicle vs unwounded 74.5 ± 6.17%). Thus a downstream consequence of MC1R-Ag treatment is reduced scarring through improved collagen deposition quality and quantity to levels approaching unwounded skin.

MC1R modulates the wound environment during healing

Wound repair from the late stages of fetal development onwards is accompanied by robust recruitment of innate immune cells to the wound. The optimal balance between sufficient leukocyte recruitment to combat any invading microorganisms versus excessive pathological inflammation which contributes to scarring, is of critical importance in any tissue repair response or therapeutic treatment *(1)*. We monitored leukocyte recruitment dynamics during dermal wound repair, finding that MC1R-Ag administration inhibits neutrophil recruitment to excisional cutaneous wounds (Fig. 2A). Surprisingly, MC1R-Ag *increased* F4/80$^+$ MΦ recruitment to day 7 wounds (Fig. 2B), however spatial analysis revealed that MΦ distribution in the skin adjacent to the wound was limited by MC1R-Ag treatment. Unlike vehicle-treated day 7 wounds where an F4/80$^+$ infiltrate is present in the wound adjacent dermis (Fig. 2C-D). MC1R-Ag treatment appears to restrict monocyte-MΦ recruitment to the wound site with little spill over. We noted no clear change in wound MΦ morphology, however, a marked improvement in erythrocyte clearance (Prussian blue$^+$ cells; Fig. 2E) was observed, along with significantly reduced wound TNFα (Fig. 2F) and oxidative stress (dihydrorhodamine$^+$ cells; Fig. 2G). Collectively, these data suggest that MC1R agonism is able to accelerate resolution

of the wound inflammatory response, possibly resulting in a shift towards the repair phase (proliferation/migration and remodelling).

Harnessing MC1R drives angiogenesis and lymphangiogenesis at sites of cutaneous repair

Angiogenesis and lymphangiogenesis are processes that principally occur either during early development or during wound repair or inflammation. Wound angiogenesis is required to enable delivery of oxygen and nutrients to the metabolically demanding repairing tissue, with impaired angiogenesis observed in aberrant healing scenarios including DFUs *(5)*. Lymphatic vessels are thought to be important in wound healing as they drain interstitial fluid to reduce tissue swelling and permit the transportation of immune cells to lymph nodes *(16)*. We therefore investigated the effect of MC1R-Ag on angiogenic and lymphangiogenic responses during cutaneous wound repair (Fig. 3). As we and others have previously shown *(17–19)*, the time course of angiogenesis preceded that of lymphangiogenesis with angiogenic sprouting occurring as early as 3 dpi, peaking at 7 dpi and vascular remodelling, including trimming of superfluous vessels occurring thereafter (Fig. 3B,D; Fig. S3). The lymphangiogenic response, however, was evident at 7 dpi, and appeared to still be ongoing at our latest time point 14 dpi (Fig. 3B). Wound treatment with MC1R-Ag profoundly enhances the angiogenic (155%) and lymphangiogenic (216%) responses with increased vessel density over vehicle-treated wounds (Fig. 3A-B). Vessel width analysis reveals that MC1R-Ag administration results in increased lymphatic vessel width but equivalent blood vessel widths in comparison to vehicle control (Fig. 3C). OCT angiography was performed to verify if the $CD31^+$ cell areas detected via immunofluorescence staining were indeed functional, perfused blood vessels. Indeed, notable, wound bed perfusion is detectable 7 dpi with MC1R-treatment and declines thereafter (Fig. 3D). To determine whether MC1R-Ag was improving wound vascularisation via direct MC1R-mediated effects on endothelial cells, we employed a microvascular endothelial cell tube formation assay. MC1R-Ag significantly increased readouts of *in vitro* angiogenesis, including total mesh area, branching interval and total segment area (Fig. 3E-G, Fig. S4). MC1R knockdown using siRNA demonstrated that these angiogenic effects of BMS-470539 are mediated by MC1R (Fig. 3F, Fig.S5). To assess wound lymphatic vasculature function, we employed an Evans Blue lymphatic drainage assay. We confirm that the observed increase in lymphatic vessel area translated to improved lymphatic drainage (Fig. 3H). Collectively, we demonstrate that BMS-470539 acts via endothelial cell MC1R to drive angiogenesis and lymphangiogenesis, resulting in improved wound bed blood supply and lymphatic drainage.

Lack of functional MC1R impairs acute wound healing

In humans and mice, lack of a functional MC1R due to spontaneous mutation, results in preferential production of the yellow-orange pigment, phaeomelanin in the skin and hair. To establish the impact of MC1R on wound healing, we generated 4 mm wounds in MC1Re/e mice, which harbour a non-functional receptor (ginger hair; C57Bl/6J background) and in wildtype (black hair; C57Bl/6J) mice. We discover that lack of functional MC1R profoundly impairs healing, with significantly delayed wound closure detectable at 1, 7, 10 and 14 dpi (Day 7 – MC1Re/e, 27.4 ± 2.1%; C57B/6J, 7.36 ± 0.83% of initial wound area; Fig. 4A-D). Scab loss, an indicator of complete reepithelialisation, is also delayed with 95% of MC1Re/e wounds retaining a scab at 7 dpi in comparison to 68.8% of wildtype control wounds (MC1Re/e + vehicle, 95 ± 5.1%; MC1Re/e + BMS-470539, 90.2 ± 6.1%; C57Bl/6J, 68.8 ± 7.84; Fig. 4E). MC1R agonist, BMS-470539, is unable to impact the wound healing response in MC1Re/e harbouring a non-functional receptor.

We have established that harnessing the MC1R using a selective agonist drives wound bed vascularisation and promotes acute wound repair. However, acute wounds typically heal without complications, therefore we asked whether this approach would be of benefit in the context of non-healing wounds.

Development of a preclinical chronic wound model

Chronic wounds represent a major unmet need and exhibit profoundly impaired wound vascularisation, which is thought to be an important determinant of wound outcome. We reasoned that administration of MC1R-Ag in a preclinical CW model would allow us to determine whether harnessing this pathway holds merit as a novel intervention for pathological healing. To get to this point, we first needed to develop a humane model that reproduces the hallmarks of human CWs, both on a macroscopic level (eg. exudate, slough, wound expansion) and a microscopic level (eg. hyperproliferative epidermis, extravasated erythrocytes, fibrinous exudate, parakeratosis). We specifically sought to develop a model that is broadly relevant across the ulcer categories of VLU, DFU and PU, rather than specifically modelling a certain category. Whilst each type of CW is associated with certain comorbidities, for example PU with conditions causing immobility; at their core they share key features. The overwhelming majority of skin ulcers develop in the over 50s, with 95 percent occurring in the over 60s. In addition, VLU, DFU and PU have been shown to exhibit high levels of wound bed oxidative stress *(3, 5, 10)*. Taking inspiration from the advantages and limitations of current murine models *(6, 7, 20, 21)*, we developed our unique model using aged animals (18-22 months) and local elevation of oxidative stress (Fig. 5A).

A 4 mm excisional wound was made to the dorsal skin of aged mice, topical Glutathione peroxidase (GPx) inhibitor, mercaptosuccinic acid (MSA) was applied, following by a transparent Tegaderm dressing (Fig. 5A). The wounds expanded into the surrounding tissue 5-fold over the first 7 dpi with the tissue taking on a macerated (white) appearance (approx. 1 dpi), followed by a thin red border appearing around the macerated area at 3 dpi but absent by 7 dpi. The wounds produced exudate and slough, stabilised at this size for the duration of the experiment (Fig.5A-B) and were well tolerated by the animals (Fig. S6). Wound architecture was compared between the well established acute excisional wound model (Fig. 5C-D), the new CW model (Fig. 5G-H) and a cohort of 44 human CWs (28 VLU, 9 DFU, 7 PU; Fig. 5E-F). During successful skin repair, at only 1 dpi a scab has formed as a result of haemostasis, reepithelialisation is not evident, provisional matrix has been deposited and a rich PMN infiltrate is notable (Fig. 5C). In contrast, at 14 dpi, reepithelialisation is complete, scab loss has occurred, few PMN remain and the wound bed is well vascularised (Fig. 5D).

In human CWs we find that fibrinous exudate, hyperproliferative epidermis, PMN infiltrate and vasculitis are consistently present, being identified in 86-100% of DFU, VLU and PU. Hypogranulosis (78-100%), extravasated erythrocytes (71-100%), parakeratosis (57-78%) and spongiosis (67-100%) were also common histomorphological features (Fig. 5E,F, Fig. S7). Hemosiderin deposition proved to be the most variable feature, found in all VLU, 56% of DFU but none observable in PU. This likely relates to specific co-morbidities including venous stasis that are most commonly found in patients with VLUs (Fig. 5E,F, Fig. S7). In our preclinical CW model, histomorphological analysis revealed a severe lack of granulation tissue formation, substantial and persistent fibrinous exudate, subcutaneous fat necrosis and presence of extravasated erythrocytes. Major disturbance to epidermal physiology was evident through hyperproliferation, spongiosis and parakeratosis, along with a complete failure of wound reepithelialisation. Whilst exudate and slough were abundant, scab formation was absent (Fig. 5G,H).

MC1R agonist rescues the healing response in a preclinical chronic wound model

In the clinic, non-healing wounds are typically managed in the community, with dressing changes and basic wound debridement performed as part of standard wound care *(22)*. Effective wound debridement is thought to partially stimulate healing, but in complex wounds, is typically insufficient to result in complete healing. To assess a potential therapeutic intervention, we therefore debrided the wounds 7 dpi (Fig. 6A,B). Topical vehicle-control and MC1R-Ag were administered in pluronic hydrogel immediately after debridement and at each subsequent dressing change 3 and 5 days later (Fig. 6A,B). Vehicle-treated wounds mimicked the hallmarks of human CWs (Fig. 6B,C), including extravasated erythrocytes, PMN infiltrate,

fibrinous exudate, spongiosis, parakeratosis and a lack of wound vascularisation (Fig. 6B,C and Fig. 5). MC1R-Ag treatment following debridement rescued the healing response. Here, we observed partial reepithelialisation, as evidenced by formation of epithelial tongues, minimal fibrinous exudate was present and a vascularised granulation tissue formed (Fig. 6B,D). Importantly, wound area and presence of wound exudate were significantly reduced with MC1R-agonist treatment (Fig. 6F,H). In contrast, MC1Re/e CWs exhibited increased wound exudate (Fig. 6E,H), NETosis, spongiosis and hemosiderin deposition, but extravasated erythrocytes were not observed (Fig. 6I)

DISCUSSION

In this study, we assessed the impact of manipulating the melanocortin 1 receptor on acute wound healing using a selective agonist, BM470539. MC1R agonism resulted in accelerated wound closure and reepithelialisation in wildtype but not MC1Re/e mice which harbour a non-functional receptor. MC1R-Ag improved wound perfusion and lymphatic drainage by promoting angiogenesis and lymphangiogenesis, reduced local oxidative stress and inflammation with a knock-on effect of reduced scarring. Our data suggest that MC1R enables wounds to transition to the proliferative phase quicker to effect efficient healing. Surprisingly we noted minimal effects on leukocyte recruitment, however, it is entirely possible that some of the impact on wound healing may be through modulating leukocyte phenotype or via leukocyte lineages out with the scope of this study. Nevertheless, MC1R-Ag acts directly on endothelial cells to drive microvascular endothelial cell sprouting and mesh formation and may therefore hold promise for pathologies characterised by poor vascularisation.

MC1R activation also has potential anti-fibrotic properties. Collagen alignment plays a significant role in scar quality, with a disordered collagen architecture being characteristic of an unwounded dermis. Using simulations and multi-scale mathematical modelling, McDougall *et al* derived equations to elucidate the molecular cause of alignment during collagen deposition. Their results suggest that a localised chemoattractant gradient, with greater effects on only those fibroblasts in the vicinity of the wound, produces a collagen pattern that is highly disordered *(23)*. This could be the driver behind reduced collagen alignment in MC1R agonist-treated wounds; macrophages were more restricted to the wound site and could thus provide localised chemoattractants. The inflammatory profile at the wound site and in the neighbouring unwounded dermis could be more comprehensively analysed for mediators known to modulate fibroblasts biology, to further elucidate the mechanism of the observed effect of MC1R-Ag on scarring.

Given that the majority of acute wounds heal without complication, and chronic wounds represent a profound and escalating burden to individuals and healthcare systems *(3)*, we sought to develop a preclinical chronic wound model to act as a platform for testing of novel interventions such as MC1R-Ag. Equally importantly, the provision of such a model has long been recognised as essential to better understand the disease process without the risk of clinical harm *(7)*. As described by Frykberg and Banks, CWs have variable underlying pathologies, including diabetes, immobility, venous stasis and can be divided into categories based on these, such as DFU, PU and VLU, however almost all CWs occur in the over 50s and exhibit elevated oxidative stress *(5)*. Whilst CWs also typically exhibit pathological alterations in the balance of various MMPs and TIMPs, manipulation of these pathways is not trivial. We therefore developed our model by combining advanced age and locally elevated oxidative stress, which proved to accurately mimic many of the hallmarks of human CWs. The model can now be used to study CW development and persistence with the view of identifying novel tractable targets for therapeutic gain.

Every preclinical model has limitations and it is important to be aware of these particularly when translating findings to the clinic. With respect to the preclinical CW model we have described here, the key considerations are concerning the differences in skin anatomy between mouse and human. In human, the epidermis and dermis are thicker and the skin is firmly adherent to the fascia. In mouse, the skin is typically not adherent to the underlying fascia, however, we note that in our model and the context of chronic inflammation, the wounds can adhere to the fascia. Indeed, others have noted a major contribution of fascia-derived fibroblasts to murine acute wound scarring, though in this scenario the wound is only temporarily adherent to fascia *(24)*. We are however encouraged by our histomorphological analysis, which revealed many of the same features of human CW epidermis, including clear hyperproliferation, spongiosis, failure to reepithelialise and parakeratosis.

The cellular and molecular mechanisms behind skin repair and scar formation and particularly development and persistence of CWs have yet to be fully elucidated, this study suggests that targeting MC1R may represent an effective strategy to rescue failed healing and reduce acute wound scarring, potentially by enabling wounds to transition to the proliferative phase quicker. We anticipate that our novel model will become a valuable tool to interrogate ulcer formation and persistence along with testing of novel interventions, whilst the discovery of MC1R agonists role in angiogenesis and lymphangiogenesis opens promising new avenues for the therapeutic exploitation of this pathway for wound healing.

MATERIALS AND METHODS

Animals

All experiments were conducted with approval from the University of Bristol or Edinburgh Local Ethical Review Committee and in accordance with the UK Home Office regulations (Guidance on the Operation of Animals, Scientific Procedures Act, 1986) under PPL PD3147DAB. C57Bl/6JCrl and MC1Re/e mice were bred in-house, maintained in conventional cages on a 12:12 light:dark cycle with *ad libitum* access to standard chow and water under a SPF environment. Animals were housed 3-5 per cage in a temperature (22-24C) and humidity controlled room. Environmental enrichment was provided in the form of dome homes, a tunnel and chew sticks. Health checks were performed on all animals prior to wounding, including baseline weight measurements, malocclusion and skin injuries due to fighting. Animals with malocclusion were excluded from the study and those with small skin injuries due to historic fighting were included providing wounds could be made without involvement of the previous injury area. Only animals that were not involved in previous procedures were used for experiments.

Aging mouse colony

Once animals reached 12 months of age, several parameters of health were monitored on a weekly basis to determine animal welfare. Parameters were weight (as compared to baseline 12 mo weight), body condition scores (as determined by visual and physical examination of each animal in accordance with the University of Edinburgh Veterinary Scientific Service guidelines) and behaviour. Weight loss of 10% and/or an increase in body condition score or evident lack of expected behaviour (interaction, movement) resulted in the animal being assessed by a vet.

Acute skin wounds

Mice (7-9 weeks old) were randomly assigned a treatment group and anaesthetized with isoflurane (Zoetis, Leatherhead, UK) by inhalation. Buprenorphine analgesia (0.05 mg/kg, s.c, Vetergesic, Amsterdam) was provided immediately prior to wounding and dorsal hair was removed using a Wahl trimmer. Four full-thickness excisional wounds were made to the shaved dorsal skin using sterile, single use 4 mm punch biopsy tools (Selles Medical, Hull, UK). Wounds were photographed with a Sony DSC-WX350 and a ruler immediately after wounding and also on days 1, 3, 7, 10 and 14 post-wounding. Vehicle (PBS) or BMS-470539 were delivered topically by pipette into the wound cavity immediately after wounding (40 μl in a 30% Pluronic F-127 gel (liquid at 4ºC, but solidifies at room temperature; Sigma Aldrich). Wound areas were calculated using ImageJ software.

Mice were housed with their previous cage mates in a 28C warm box (Scanbur, Denmark) overnight following wounding, with paper towels used as bedding to avoid sawdust entering the open wounds. Dome home entrances were enlarged to prevent animals scraping their dorsal skin wounds. Animals were moved into clean conventional cages at 22-24C the following morning.

Chronic skin wounds

Mice (18 months) were randomly assigned a treatment group and anaesthetized with isofluorane and placed on a heated mat to maintain body temperature. Buprenorphine analgesia (0.05 mg/kg, s.c, Vetergesic, Amsterdam) was provided immediately prior to wounding and dorsal hair was removed using a BaByliss trimmer. Nair cream (Church and Dwight, Folkestone, UK) was used to remove the remnants of the dorsal hair to create a surface that the Tegaderm dressing would adhere to. Depilatory cream was carefully removed using PBS and tissue paper to avoid chemical irritation. Claws were trimmed to minimise the potential for scratch-induced skin trauma during the protocol. A single 4 mm excisional wound (Selles Medical, UK) was made to the cranial dorsal skin near the shoulder blades. A suspension of mercaptosuccinic acid (MSA, 400 mg/kg, Sigma-Aldrich) in 40% Pluronic hydrogel was prepared and 25 μl administered topically into the wound. Wounds were dressed with a sterile Tegaderm dressing (3M, Bracknell, UK) which prevented wound contamination, maintained a moist environment and ensure animals would not clean their wounds. Bepanthen Ointment (Bayer, Reading, UK) was applied to the uncovered, depilated skin surrounding the dressing to minimise any irritation.

Mice were individually housed in conventional cages in a 28C warm box throughout the experiment, with additional bedding, which effectively enabled these elderly mice to maintain their body weight. Animals were provided with ‘mash’ (standard chow rehydrated in sterile water) throughout the protocol. Mice were monitored as outlined in Fig. S6.

At Day 7 post-wounding, CWs were carefully debrided to remove dead and sloughing tissue. Briefly, mice were anaesthetized with isoflurane by inhalation, placed on a heated mat and administered Buprenorphine (0.05 mg/kg sc). The existing Tegaderm dressing was carefully removed, ensuring the wound was not pulled in the process. Debridement was performed using 4.25 inch dissection scissors and curved tweezers (Sigma-Aldrich)

Vehicle (PBS) or BMS-470539 (MC1R-Ag) were delivered topically by pipette into the wound cavity immediately after debridement (100 μl in a 30% Pluronic F-127 gel; Sigma Aldrich). Wound areas were calculated using ImageJ software.

BMS-470539

MC1R agonist, BMS-470539, was synthesised by Mimotopes (Minneapolis, USA), reconstituted (1 mM in PBS + 0.1% BSA) and stored at -80°C for up to 6 months. BMS-470539 was diluted from fresh aliquots for each experiment.

Evans Blue assay of lymphatic drainage

Evans blue dye (Sigma-Aldrich, Poole) was dissolved in sterile saline solution to a concentration of 0.5% w/v and 10 μl was injected into the cutaneous wound bed 8 hours prior to cull. The gross appearance of the tissue was recorded using a digital camera immediately following cull. The skin draining lymph nodes (axillary, brachial and inguinal) were then harvested into 200 μl of formamide and incubated for 24 h at 55°C to extract the dye. The tissue pieces were discarded, debris removed via centrifugation and absorbance read in triplicate at 610 nm.

Wound processing

Acute wounds were harvested on days 1, 3, 7, 10 and 14 post-wounding, fixed in 4% PFA (overnight at 4C on a rocker, Sigma Aldrich), washed 3 x 5 min in PBS, transferred to 70% ethanol and then embedded in paraffin. Day 1 and 3 wounds were cut in half using a scalpel and sections (10 µm) taken from the middle of the wound. Day 7, 10 and 14 wounds were sectioned through the wound beyond the midpoint and wound centres identified by staining with Haematoxylin (Gills No.3) and Eosin (Sigma). All chronic wounds were bisected.

Histology

FFPE sections were deparaffinised and rehydrated in: xylene (2 x 3 min), 100% ethanol (2 x 3 nub), 90% ethanol (3 min) and 70% ethanol (3 min). Sections were placed in running tap water before being submerged in haematoxylin (Sigma-Aldrich, Dorset, UK) for 5 s – 1 min depending on staining intensity desired. Excess haematoxylin was rinsed off in tap water twice. Slides were then briefly submerged in acid alcohol (300 ml dH20, 700 ml 100% ethanol, 3 ml concentrated HCL; Sigma-Aldrich), followed by tap water wash. Sections were submerged in eosin (Sigma-Adrich) for 30 s to provide a counterstain to the haematoxylin. After tap water washes (x 3), sections were dehydrated for mounting in sequential baths of 70%, 90%, 100% ethanol and xylene (x 2) for 30 seconds each. DPX mountant (Sigma-

Aldrich) was applied to the sections and a Menzel microscope coverslip applied (25 x 60 mm, 0.13 mm thick; Thermfisher Scientific, Renfrew, UK). For Picrosirius Red (PSR) staining for collagen, the above protocol was followed but with PSR (0.5 g Sirius Red, 1.3% picric acid in dH2O; Sigma-Aldrich) for 1 hour and no eosin counterstain. For Prussian Blue staining, the above protocol was followed but with Prussian Blue (10% HCl, 5% potassium ferrocyanide in dH2O used rather than haematoxylin.

Immunohistochemistry

Skin sections were deparaffinised and rehydrated as described above. Sections were encircled with a hydrophobic barrier using an ImmEdge pen (Vector labs, Peterborough, UK). Antigen retrieval was carried out using Proteinase K (5 μg/ml, 7 mins, Dako, UK). Sections were rinsed in running tap water for 5 min, blocked (1% BSA, 0.1% Gelatin, 0.5% Triton X-100; Sigma-Aldrich) for 30 min at room temperature. Sections were incubated in primary antibody diluted in block, overnight at 4C in a humidified chamber. After PBS-0.1% Tween-20 wash, an ImmPRESS polymer detection kit was used, followed by a DAB kit, as per the manufacturer's instructions (Vector labs). Sections were counterstained with haematoxylin, dehydrated and mounted as described above.

Microscopy

Tissue sections were imaged on an Axioscan Z1 slide scanner (Zeiss, Cambridge, UK) using the 20x air objective. Immunofluorescence images were taken using a Leica DM2500 microscope, Leica DFC7000 camera and LAS software (Leica Microsystems, GmbH, Milten Keynes, UK), using the 20 x air objective. Numbers of leukocytes per field of view (FOV) were calculated using thresholded 32-bit images and the “analyze particles” function in FIJI software. Blood and lymphatic vessels were quantified by thresholding on fluorescent area in FIJI software.

Collagen alignment

Collagen fibre orientation was desired to be able to identify the level to which wounds recovered their natural structural components during the wound healing process. To undertake this, we developed a MATLAB code which first isolated collagen fibrils from non-fibrous tissue using a colour-based segmentation algorithm. First, the user selected image is converted from an RGB image to a two-dimensional matrix of type $m \times n \times 3$. Where m and n represent the row and column indices respectively. Our code (which we name FIBRAL) converts the image colour space from RGB to L*a*b to more accurately predict small colour differences, key for PSR staining in which small variation detection is required *(25)*. Both the full a-channel and positive range of the b-channel were isolated and superimposed. This new

matrix was transformed into grayscale with contrast and brightness increased by 20% and 5% respectively.

To determine the spatial distribution of collagen fibres, a two-dimensional Fourier transformation was performed on the image. This data was transformed from cartesian to polar coordinates by grouping predominant frequency-component orientations of the fibres in 1-degree increments from 0 to 180 degrees. The total intensity at each angle was calculated by summing the grayscale intensity values of each pixel contained within the group. Large intensity values represented the summation of multiple sinusoidal waves with large amplitude signifying major fibre alignment along the respective orientation. From this data, a comparative analysis can be conducted whereby the dot product was calculated using each permutation of resulting vectors (parallel vectors would provide a dot product of 1, with orthogonal vectors presenting a dot product value of -1). All results were normalised to lie between 0 and 1 with a directionality quotient of 1 representing a parallel field of fibres and a directionality quotient of 0 representing full fibre orientation across all angles in the tissue. The code was validated against images with dominant fibre orientations and combinations thereof. Full details of the coding approach are included in the supplementary material.

Wound Optical Coherence Tomography Angiography

OCTA imaging is a non-invasive imaging method which utilises light to produce cross-sectional images of tissue architecture *in situ* and in real time. This form of imaging allowed the tracking of wound healing parameters such as reepithelialisation within a single mouse over a time course of healing. Additionally OCTA provides information on the perfusion of new blood vessels which cannot be obtained utilising other methods such as immunofluorescence staining.

Equipment used in this study were designed and developed by Professor Zhihong Huang, Dr. Kanheng Zhou, Mr. Yubo Ji and Mr. Duo Zhang (University of Dundee *(26, 27)*). Mice were anaesthetised at the indicated time points place on a heatpad and ultrasound transmission gel (Anagel, Ana Wiz Ltd, Surrey, UK) was applied between the OCT probe and wound to enhance refractive index coupling. A clinical prototype handheld OCTA system was utilised to image dorsal skin wounds. A 200-kHz vertical-cavity surface-emitting swept source laser (5 mW) (SL132120, Thorlabs Inc., Newton, USA) was used as the light source in the system paired with a XY galvo-scanner (6210H, Cambridge technology, Bedford, USA) and a 5X objective lens (LSM03, Thorlabs Inc., Newton, USA). With this configuration, the handheld probe provided a scanning range of 10 × 10 mm2. To generate high resolution 3D OCTA images for skin architecture and vasculature, the following B-M scanning protocol was applied:

Firstly, A-lines were acquired consecutively with a 10 μm interval along the fast scanning axis to generate a B-frame. Each B-frame was then repeated four times at the same location for blood flow extraction. Next, the described repeated B-scans were looped consecutively along the slow scanning axis also with a 10 μm interval to form a complete 3D volume scan. The final volumetric dataset comprised 600 A-lines and 600 cross-sectional planes (2400 B-frames). Data was collected through a customised LabVIEW (NI, Texas, USA) interface for processing.

HMEC-1 culture and transfection

HMEC-1 cells (ATCC: CRL-3243) were cultured in EGM-2 MV (EBM-2 added with growth factors and other supplements, PromoCell). Lipofectamine RNAiMAX (Thermo Fisher Scientific) was used to transfect HMEC-1 with siRNA control or siRNA MC1R oligonucleotides (Qiagen) (20 nM final concentration).

Endothelial Tube Formation Assay

Matrigel (50 µL/well) (BD Matrigel Basement Membrane Matrix, BD Biosciences) was added to the wells in a 96-well plate and allowed to polymerize at 37 °C for 30 min. HMEC-1 cells, an immortalised human microvascular endothelial cell line *(28)* (15,000 cells) previously transfected with siRNA-control or siRNA MC1R were added to the top of the Matrigel and treated with MC1R agonist BMS-470539. After incubation for 8 hr, tube formation was assessed by acquiring four randomly microscopic fields (magnification ×10) by using Nikon Eclipse Ti inverted microscope. Total tube length and branching points were assessed by Angiogenesis Analyzer for ImageJ analysis software *(29)*. For confocal imaging, cells were fixed (4% PFA, 15 m), blocked ( ) and stained (phalloidin, ; DAPI,)

Human Tissue

FFPE sections of human chronic wounds were provided by NHS Lothian Tissue Bank (ethical approval: 15/ED/0094) with approval from the Tissue Governance Committee (2017/0023/SR736). Inclusion criteria were pressure ulcers, diabetic foot ulcers and venous leg ulcers from male and female donors over 50 years of age. Exclusion criteria were patients with cancer, pressure ulcers from patients with diabetes. Prior to receipt, all samples were anonymised.

Statistical analysis

Student's *t*-test, one-way and two-way ANOVA with Bonferroni's multiple comparison test were performed using GraphPad Prism 9.0 software and detailed in the respective Figure legends.

Diagrams

Biorender was used to create the schematics in Figures 1, 5 and 6.

Acknowledgments: We acknowledge the support of the QMRI SURF facilities for histological services and BVS (Bioresearch and Veterinary Services), especially Dr Nacho Vinuela-Fernandez for assistance with animal studies. We thank Professor Ian Jackson for providing the MC1Re/e mouse line and Dr Andrew Tambyraja and Professor Keith Harding for helpful insights on chronic wounds from a clinical perspective and Professor Paul Martin for general discussions. We thank Dr Alison Munro of the Institute of Genetics and Cancer (IGC) for running nanostring assays and Wolfson Bioimaging Facility for assistance with Incucyte experiments. Thanks also to Prof Stuart Forbes, Prof David Dockrell and Prof Julia Dorin for mentorship.

Funding: This work was funded by a Sir Henry Dale Fellowship (202581/Z/16/Z), Elizabeth Blackwell Early Career Fellowship (Wellcome ISSF) and a University of Edinburgh Chancellors Fellowship awarded to Dr Jenna L Cash. Dr Holly Rocliffe was supported with a Chancellors Fellowship PhD Studentship.

Contributions: HR and SAW performed experiments, analysed the data and wrote the manuscript. GK and AP performed experiments and analysed the data. YN performed histology and histological analysis of skin wounds. KZ and YJ performed OCT imaging and analysis under the supervision of ZH. CB developed FIBRAL under the supervision of MC). AP performed experiments and analysed data. TZ performed vessel width analysis. AC advised on the design and execution of *in vitro* angiogenesis experiments, performed and analysed these experiments. JLC conceived and planned the project, performed the experiments, analysed and interpreted the data, wrote the manuscript, obtained funding, and supervised the project.

Figure 1. MC1R drives wound healing with reduced scarring
Four 4 mm excisional wounds were made to the dorsal skin of C57Bl/6J mice. Vehicle (PBS) or MC1R agonist (BMS-470539) in 30% Pluronic hydrogel was administered topically into the wound immediately after wounding.

(A) Schematic diagram illustrating the location of acute skin wounds (top) and heatmap showing the z-transformed expression values of indicated genes in whole wounds at days 0, 1, 3 and 7 dpi normalised to unwounded 8 w old skin (bottom). Five animals per group, two independent experiments.
(B) Representative macroscopic photos of vehicle- and MC1R agonist-treated wounds 0-14 dpi
(C) Longitudinal macroscopic quantification of wound areas at 1, 3, 7, 10 and 14 dpi in 8 w old mice in relation to their respective initial size at 0 dpi. n = 7 biological replicates for each group from three independent experiments.
(D) Epithelial tongue length at 3 dpi. 9 wounds (vehicle) and 10 wounds (MC1R-ag).
(E) Heatmap generated from OCT-derived images illustrating epidermal thickness immediately around the wound at 3 and 5 dpi, and in the wound bed at 7, 10 and 14 dpi. 6 wounds per group.
(F) Quantification of epidermal thickness at 7 dpi, with 7 (vehicle) and 11 (MC1R-Ag) wounds per group.
(G) Scab presence 1-14 dpi. n = 7 biological replicates for each group from three independent experiments.
(H) Representative H&E-stained wound mid-sections at 7 dpi illustrating scab loss and smaller wound area in MC1R-agonist treated wounds.
(I) Picrosirius red-stained unwounded skin and wound mid-sections at 7 dpi. Lpf (left), hpf (right).
(J) Collagen alignment (top) and area (bottom) in unwounded skin and 7 dpi wounds, with 7 (vehicle) and 11 (MC1R-Ag) wounds per group. See Fig. S2.
(K) Polar plots illustrating collagen fiber alignment in unwounded skin and wounds at 7 dpi.

Data are expressed as mean ± SEM. * $p<0.05$, ** $p<0.01$, *** $p<0.001$ by two-way ANOVA with Bonferroni's multiple comparison test (C, G, J) or Student's unpaired t test (D, F) relative to vehicle-treated wounds.

Figure 2. MC1R agonist modules the wound microenvironment
Four 4 mm excisional wounds were made to the dorsal skin of C57Bl/6J mice. Vehicle (PBS) or MC1R agonist (BMS-470539) in 30% Pluronic hydrogel was administered topically into the wound immediately after wounding.
(A) Quantification of wound bed neutrophil recruitment ($Ly6G^+$ cell) 1-7 dpi.
(B) Quantification of wound be monocyte-macrophage recruitment ($F4/80^+$ cell) 3-14 dpi.
(D) Macrophage immunostaining (F4/80) through the mid-point of wounds 7 dpi.
(E) Quantification of macrophage distribution across wounds and adjacent tissue.
(F) Representative hpf and quantification of Prussian $blue^+$ iron-loaded cells within the wound 3-14 dpi. Images from 7 dpi sections with Eosin counterstain.
(G) Quantification and representative lpf of TNFα expression (brown) with haematoxylin counterstain.
(H) Representative hpf and quantification of oxidative stress ($dihydrorhodamine^+$ pixel area; green). Second harmonic generation (SHG; collagen, white).
Data are expressed as mean ± SEM. * $p<0.05$, ** $p<0.01$, *** $p<0.001$ by two-way ANOVA with Bonferroni's multiple comparison test (A, B, E, F) or Student's unpaired t test (G) relative to vehicle-treated wounds. Seven to eleven wounds per group from three independent experiments.

Figure 3. MC1R agonist drives wound angiogenesis and lymphangiogenesis
Four 4 mm excisional wounds were made to the dorsal skin of C57Bl/6J mice. Vehicle (PBS) or MC1R agonist (BMS-470539) in 30% Pluronic hydrogel was administered topically into the wound immediately after wounding.

(A) Representative CD31 (magenta) and Lyve-1 (yellow) immunostaining of vehicle- and MC1R agonist-treated wounds at 7 dpi (vehicle, n=6; MC1R agonist, n=5 per treatment group from three independent experiments).
(B) Quantification of $CD31^+$ (blood vessel) area and Lyve-1^+ (lymphatic vessel) area per hpf. See also Fig. S3.
(C) Blood vessel and lymphatic vessel width quantification per hpf. Vehicle (1370 blood vessels, 38 lymphatic vessels, 6 biological replicates), MC1R agonist (1286 blood vessels, 54 lymphatic vessels, 5 biological replicates).
(D) OCT angiography of blood flow demonstrating functionality of vessels, along with corresponding structural image 7, 10 and 14 dpi. Red line demarcates wound edge.
(E) Representative images of Matrigel angiogenesis assay with HMEC-1 cells treated with vehicle or MC1R agonist BMS-470539 (250 nM). Cells stained with Phalloidin (magenta) and DAPI (blue).
(F) An example of changes in one *in vitro* angiogenesis parameter, 'Total segment length' in the presence and absence of MC1R agonist (250 nM and 850 nM), control siRNA and MC1R siRNA. Three independent experiments, each with five technical replicates. See also Fig. S5.
(G) Percentage change in *in vitro* angiogenesis parameters with MC1R agonist-treatment (850 nM BMS-470539) relative to vehicle-treated control. Four independent experiments. See also Fig. S4.
(H) Quantification and representative macroscopic photos of skin-draining lymph nodes of mice 10 dpi, where Evans blue was injected into the wound bed to assess lymphatic drainage capacity of wounds treated with vehicle control or MC1R agonist at 0 dpi.

Data are expressed as mean ± SEM. * $p<0.05$, ** $p<0.01$ by two-way ANOVA with Bonferroni's multiple comparison test (B,F) or Student's unpaired t test (C,H) relative to vehicle-treated wounds.

Figure 4. Lack of functional MC1R impairs acute wound healing

Four 4 mm excisional wounds were made to the dorsal skin of MC1Re/e and C57Bl/6J mice. Vehicle (PBS) or MC1R agonist (BMS-470539) in 30% Pluronic hydrogel was administered topically into the wound immediately after wounding.

(A) Representative macroscopic photos of vehicle- and BMS-470539-treated wounds in MC1Re/e mice in comparison to C57Bl/6J vehicle-treated wounds (also see Fig. 1B).
(B) Longitudinal macroscopic quantification of wound areas in MC1Re/e and Wildtype mice at 1, 3, 7, 10 and 14 dpi.
(C) Wound area at 7 dpi in C57Bl/6J and MC1Re/e mice.
(D) Representative H&E-stained wound mid-sections at 7 dpi in MC1Re/e and wildtype mice. Epidermal tongues highlighted in yellow.
(E) Scab presence 0-14 dpi in MC1Re/e and wildtype mice

Data are expressed as mean ± SEM. ** $p<0.01$, *** $p<0.001$ by two-way ANOVA with Bonferroni's multiple comparison test (B,E) or Student's unpaired t test (C) relative to C57Bl/6J wounds. 5 MC1Re/e + vehicle, 5 MC1Re/e + BMS-470539 and 8 C57Bl/6J + vehicle-treated animals per group from 2 independent experiments.

Figure 5. Preclinical model recapitulates key features of human chronic wounds

(A) Top - Schematic diagram detailing the method used to create chronic wounds in aged animals (>18 months). A single 4 mm excisional wound was made to the upper dorsal skin of 18-22 m old C57Bl/6J mice. Mercaptosuccinic acid suspended in 40% Pluronic hydrogel was topically administered to the wound immediately after injury, followed by placement of a Tegaderm wound dressing. Dressing was changed at 7, 10 and 12 dpi and wound harvest at 14 dpi. Bottom – Macroscopic photos showing chronic wound development from 0 –14 dpi.

(B) Longitudinal macroscopic quantification of wound areas at 1, 3, 7, 10 and 14 dpi in acute (young 8 w old mice; n=8) and age-impaired (18-24 m old mice; n=8) healing versus chronic non-healing wounds (n=15 at 14 dpi, n=8 at 7 and 10 dpi). Data expressed as mean ± SEM, **** $p<0.0001$.
(C) Representative low power field (lpf) **mouse acute wound** H&E-stained section at 1 dpi (n=8 biological replicates) with key histological features shown below in high power field (hpf).
(D) Representative low power field (lpf) **mouse acute wound** H&E-stained section at 14 dpi (n=8 biological replicates) with key histological features shown below in high power field (hpf).
(E) Representative lpf **human chronic wound** H&E-stained section (n=44 patients) with key histological features shown below in hpf.
(F) Radar plot indicating mean prevalence (%) of key chronic wound features observed in human DFU (n=9), VLU (n=28) and PU (n=7).
(G) Representative lpf **mouse chronic wound** H&E-stained sections at 14 dpi with key histological features shown below in hpf. n=10 biological replicates from 3 independent experiments.
(H) Radar plot indicating mean prevalence (%) of key chronic wound features observed in human chronic wounds (DFU, VLU and PU, n=44), in comparison to the murine preclinical chronic wound model (n=10).

Red arrow heads indicate wound margins.

Figure 6. MC1R agonist rescues the healing response in a preclinical chronic wound model

(A) Schematic diagram detailing the chronic wound protocol from wound debridement through to harvest. Wounds were debrided of devitalised tissue 7 dpi, with dressing changes and topical delivery of vehicle control or MC1R agonist in 30% Pluronic hydrogel at 7, 10 and 12 dpi and wound harvest at 14 dpi.
(B) Representative macroscopic photos showing chronic wounds immediately before and after debridement at 7 dpi, then at 10 and 14 dpi with topical vehicle- or MC1R agonist-treatment. MC1Re/e mice received identical treatment to vehicle-treated C57Bl/6J animals.

(C-E) Representative lpf H&E-stained sections at 14 dpi with key histological features shown below in hpf. (C) Vehicle-treated chronic wound in C57Bl/6J mouse, (D) MC1R agonist-treated chronic wound in C57Bl/6J mouse, (E) Vehicle-treated chronic wound in MC1Re/e mouse. Red arrow heads mark wound edges (C-E), tissue above the black dashed lines is fibrinous exudate (C,E). Yellow lines mark epithelial tongues (D). fn, fat necrosis.

(F) Quantification of wound areas at 10, 12 and 14 dpi, normalised to 7 dpi areas. ** $p<0.01$ relative to Vehicle + debridement. # $p<0.05$ relative to No debridement group.
(G) Radar plot indicating mean prevalence (%) of key histomorphological features in vehicle and MC1R agonist-treated chronic wounds.
(H) Stacked bar graph indicating prevalence of chronic wounds with visible wound exudate.
(I) Radar plot indicating mean prevalence (%) of key histomorphological features in C57Bl/6J and MC1Re/e chronic wounds.

C57Bl/6J chronic wounds with no debridement (n=6), with debridement and vehicle-treatment (n=7), with debridement and MC1R agonist-treatment (n=5). MC1Re/e chronic wounds with no debridement (n=7) from three independent experiments.

References

1. J. L. Cash, P. Martin, Myeloid Cells in Cutaneous Wound Repair. , 17 (2016).

2. M. Rodrigues, N. Kosaric, C. A. Bonham, G. C. Gurtner, Wound Healing: A Cellular Perspective. *Physiological Reviews* **99**, 665–706 (2019).

3. C. K. Sen, G. M. Gordillo, S. Roy, R. Kirsner, L. Lambert, T. K. Hunt, F. Gottrup, G. C. Gurtner, M. T. Longaker, Human skin wounds: A major and snowballing threat to public health and the economy. *Wound Repair and Regeneration* **17**, 763–771 (2009).

4. M. Olsson, K. Järbrink, U. Divakar, R. Bajpai, Z. Upton, A. Schmidtchen, J. Car, The humanistic and economic burden of chronic wounds: A systematic review: The burden of chronic wounds. *Wound Rep and Reg* **27**, 114–125 (2019).

5. R. G. Frykberg, J. Banks, Challenges in the Treatment of Chronic Wounds. *Advances in Wound Care* **4**, 560–582 (2015).

6. R. Nunan, K. G. Harding, P. Martin, Clinical challenges of chronic wounds: searching for an optimal animal model to recapitulate their complexity. *Disease Models & Mechanisms* **7**, 1205–1213 (2014).

7. J. K. Zindle, E. Wolinsky, K. M. Bogie, A review of animal models from 2015 to 2020 for preclinical chronic wounds relevant to human health. *Journal of Tissue Viability* **30**, 291–300 (2021).

8. S. R. Nussbaum, M. J. Carter, C. E. Fife, J. DaVanzo, R. Haught, M. Nusgart, D. Cartwright, An Economic Evaluation of the Impact, Cost, and Medicare Policy Implications of Chronic Nonhealing Wounds. *Value in Health* **21**, 27–32 (2018).

9. K. Moore, E. Huddleston, M. C. Stacey, K. G. Harding, Venous leg ulcers ? the search for a prognostic indicator. *Int Wound Journal* **4**, 163–172 (2007).

10. O. Q. Goh, G. Ganesan, N. Graves, Y. Z. Ng, K. Harding, K. B. Tan, Incidence of chronic wounds in Singapore, a multiethnic Asian country, between 2000 and 2017: a retrospective cohort study using a nationwide claims database. *BMJ Open* **10**, e039411 (2020).

11. L. A. Muffley, K. Q. Zhu, L. H. Engrav, N. S. Gibran, A. M. Hocking, Spatial and Temporal Localization of the Melanocortin 1 Receptor and Its Ligand α–Melanocyte-Stimulating Hormone during Cutaneous Wound Repair. *J Histochem Cytochem.* **59**, 278–288 (2011).

12. P. Valverde, E. Healy, I. Jackson, J. L. Rees, A. J. Thody, Variants of the melanocyte–stimulating hormone receptor gene are associated with red hair and fair skin in humans. *Nat Genet* **11**, 328–330 (1995).

13. R. F. Sood, A. M. Hocking, L. A. Muffley, M. Ga, S. Honari, A. P. Reiner, A. Rowhani-Rahbar, N. S. Gibran, Race and Melanocortin 1 Receptor Polymorphism R163Q Are Associated with Post-Burn Hypertrophic Scarring: A Prospective Cohort Study. *Journal of Investigative Dermatology* **135**, 2394–2401 (2015).

14. G. Leoni, M.-B. Voisin, K. Carlson, S. Getting, S. Nourshargh, M. Perretti, The melanocortin MC1 receptor agonist BMS-470539 inhibits leucocyte trafficking in the inflamed vasculature: Melanocortins control vascular inflammation. *British Journal of Pharmacology* **160**, 171–180 (2010).

15. J. Lorenz, E. Seebach, G. Hackmayer, C. Greth, R. J. Bauer, K. Kleinschmidt, D. Bettenworth, M. Böhm, J. Grifka, S. Grässel, L. Malaval, Ed. Melanocortin 1 Receptor-Signaling Deficiency Results in an Articular Cartilage Phenotype and Accelerates Pathogenesis of Surgically Induced Murine Osteoarthritis. *PLoS ONE* **9**, e105858 (2014).

16. E. Güç, P. S. Briquez, D. Foretay, M. A. Fankhauser, J. A. Hubbell, W. W. Kilarski, M. A. Swartz, Local induction of lymphangiogenesis with engineered fibrin-binding VEGF-C promotes wound

healing by increasing immune cell trafficking and matrix remodeling. *Biomaterials* **131**, 160–175 (2017).

17. K. Paavonen, P. Puolakkainen, L. Jussila, T. Jahkola, K. Alitalo, Vascular Endothelial Growth Factor Receptor-3 in Lymphangiogenesis in Wound Healing. *The American Journal of Pathology* **156**, 1499–1504 (2000).

18. J. M. Rutkowski, K. C. Boardman, M. A. Swartz, Characterization of lymphangiogenesis in a model of adult skin regeneration. *American Journal of Physiology-Heart and Circulatory Physiology* **291**, H1402–H1410 (2006).

19. D. B. Gurevich, C. E. Severn, C. Twomey, A. Greenhough, J. Cash, A. M. Toye, H. Mellor, P. Martin, Live imaging of wound angiogenesis reveals macrophage orchestrated vessel sprouting and regression. *EMBO J* **37** (2018), doi:10.15252/embj.201797786.

20. S. Dhall, D. Do, M. Garcia, D. S. Wijesinghe, A. Brandon, J. Kim, A. Sanchez, J. Lyubovitsky, S. Gallagher, E. A. Nothnagel, C. E. Chalfant, R. P. Patel, N. Schiller, M. Martins-Green, V. D. Appanna, Ed. A Novel Model of Chronic Wounds: Importance of Redox Imbalance and Biofilm-Forming Bacteria for Establishment of Chronicity. *PLoS ONE* **9**, e109848 (2014).

21. S. Dhall, D. C. Do, M. Garcia, J. Kim, S. H. Mirebrahim, J. Lyubovitsky, S. Lonardi, E. A. Nothnagel, N. Schiller, M. Martins-Green, Generating and Reversing Chronic Wounds in Diabetic Mice by Manipulating Wound Redox Parameters. *Journal of Diabetes Research* **2014**, 1–18 (2014).

22. J. F. Guest, G. W. Fuller, P. Vowden, Cohort study evaluating the burden of wounds to the UK's National Health Service in 2017/2018: update from 2012/2013. *BMJ Open* **10**, e045253 (2020).

23. S. McDougall, J. Dallon, J. Sherratt, P. Maini, Fibroblast migration and collagen deposition during dermal wound healing: mathematical modelling and clinical implications. *Phil. Trans. R. Soc. A.* **364**, 1385–1405 (2006).

24. D. Jiang, S. Christ, D. Correa-Gallegos, P. Ramesh, S. Kalgudde Gopal, J. Wannemacher, C. H. Mayr, V. Lupperger, Q. Yu, H. Ye, M. Mück-Häusl, V. Rajendran, L. Wan, J. Liu, U. Mirastschijski, T. Volz, C. Marr, H. B. Schiller, Y. Rinkevich, Injury triggers fascia fibroblast collective cell migration to drive scar formation through N-cadherin. *Nat Commun* **11**, 5653 (2020).

25. D. J. Bora, A. K. Gupta, F. A. Khan, Comparing the Performance of L*A*B* and HSV Color Spaces with Respect to Color Image Segmentation (2015) (available at http://arxiv.org/abs/1506.01472).

26. Y. Ji, S. Yang, K. Zhou, J. Lu, R. Wang, H. R. Rocliffe, A. Pellicoro, J. L. Cash, C. Li, Z. Huang, Semisupervised representative learning for measuring epidermal thickness in human subjects in optical coherence tomography by leveraging datasets from rodent models. *J. Biomed. Opt.* **27** (2022), doi:10.1117/1.JBO.27.8.085002.

27. Y. Ji, S. Yang, K. Zhou, H. R. Rocliffe, A. Pellicoro, J. L. Cash, R. Wang, C. Li, Z. Huang, Deep-learning approach for automated thickness measurement of epithelial tissue and scab using optical coherence tomography. *J. Biomed. Opt.* **27** (2022), doi:10.1117/1.JBO.27.1.015002.

28. E. W. Ades, F. J. Candal, R. A. Swerlick, V. G. George, Susan. Summers, D. C. Bosse, T. J. Lawley, HMEC-1: Establishment of an Immortalized Human Microvascular Endothelial Cell Line. *Journal of Investigative Dermatology* **99**, 683–690 (1992).

29. G. Carpentier, S. Berndt, S. Ferratge, W. Rasband, M. Cuendet, G. Uzan, P. Albanese, Angiogenesis Analyzer for ImageJ — A comparative morphometric analysis of “Endothelial Tube Formation Assay” and “Fibrin Bead Assay.” *Sci Rep* **10**, 11568 (2020).

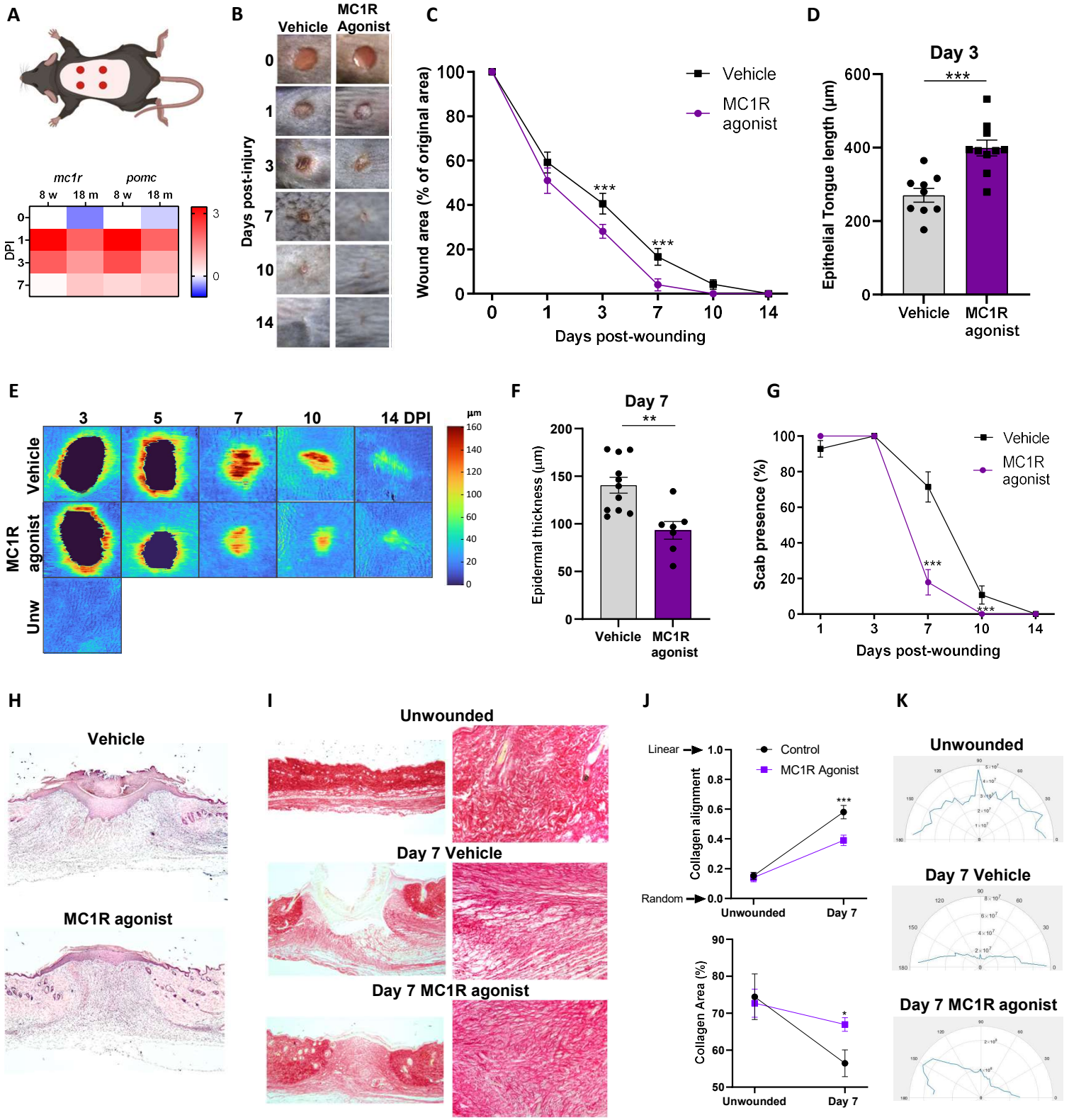

Figure 1 – MC1R drives wound healing with reduced scarring

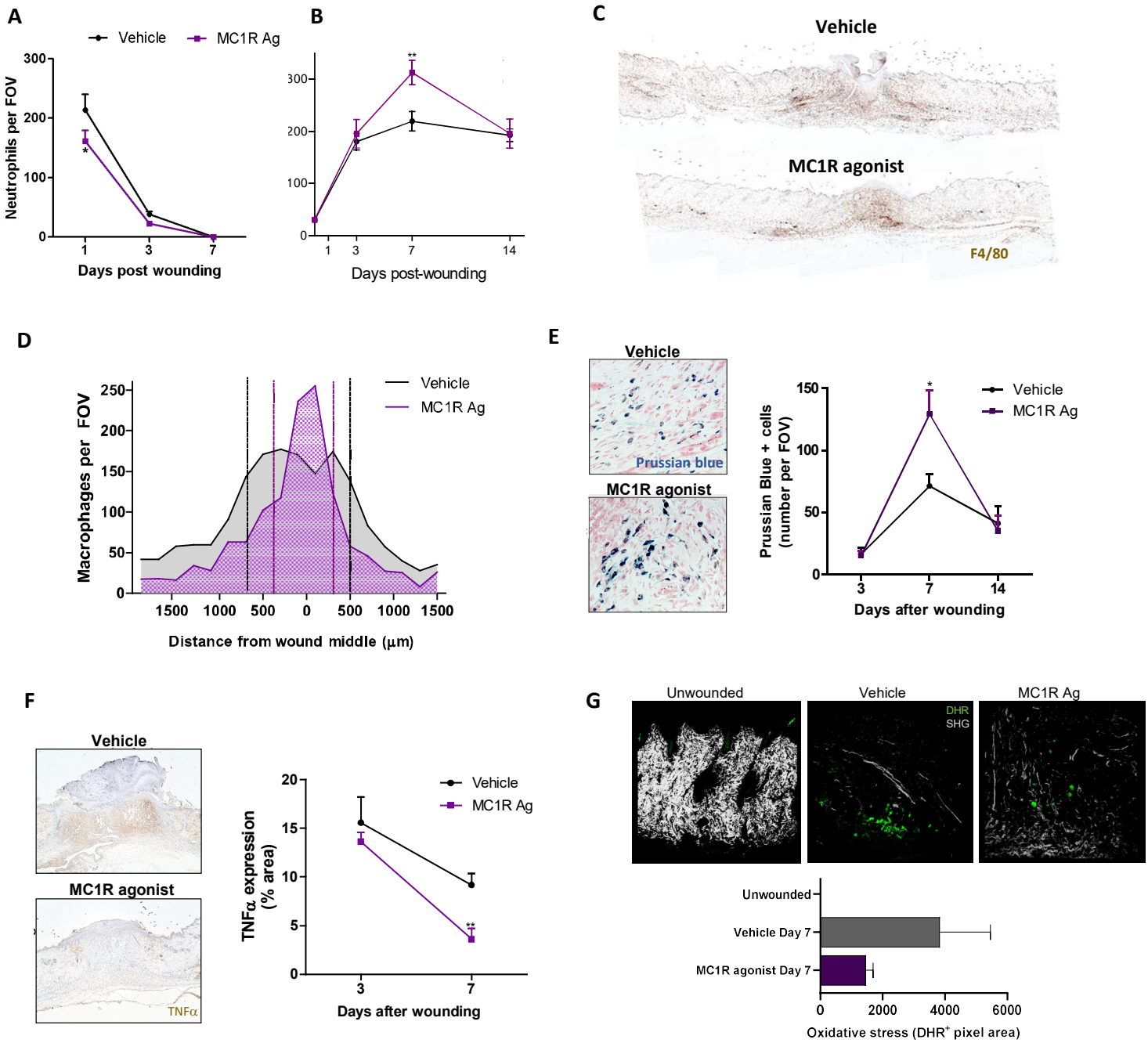

Figure 2 – MC1R agonist modulates wound microenvironment

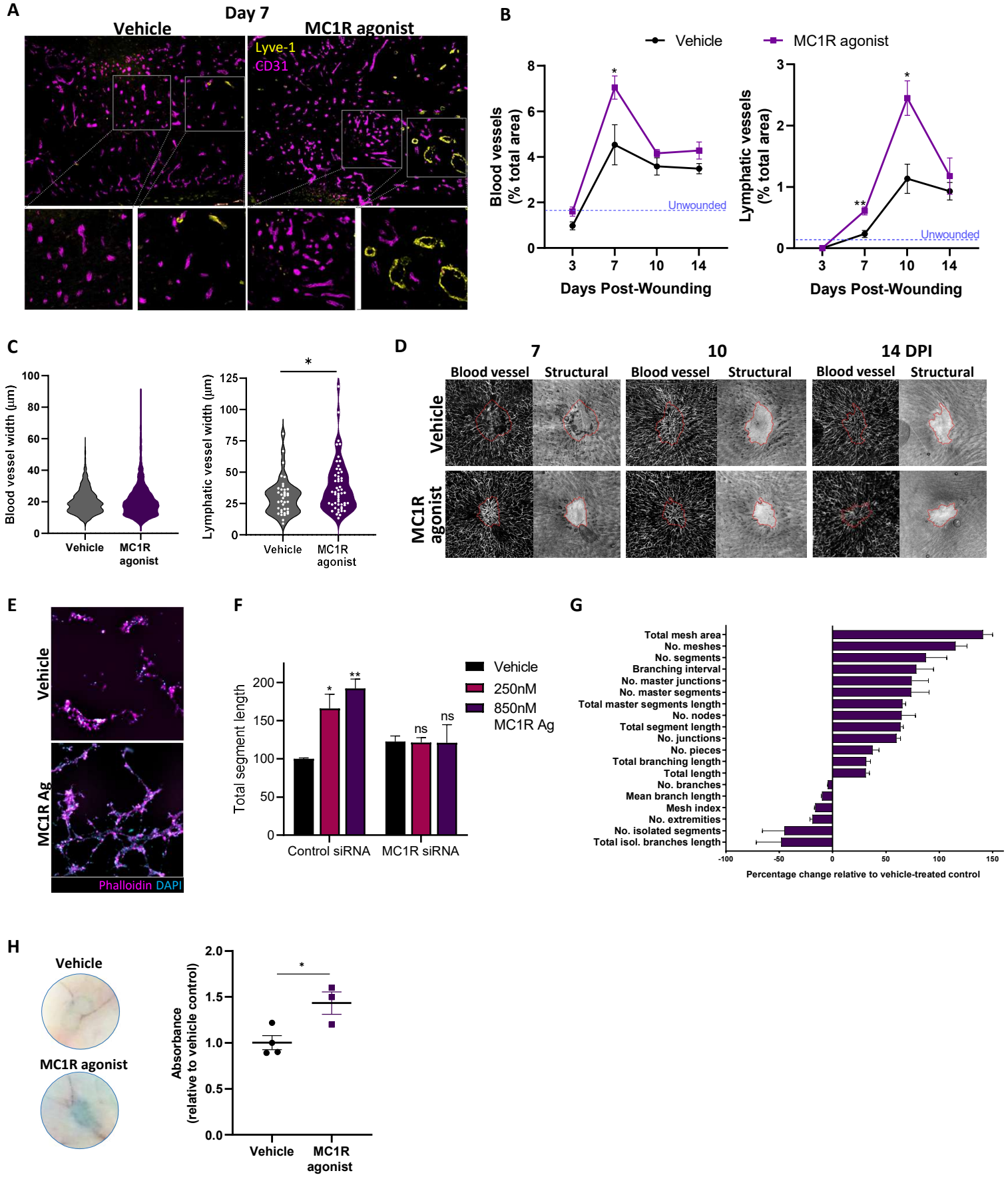

Figure 3 – MC1R agonist drives wound angiogenesis and lymphangiogenesis

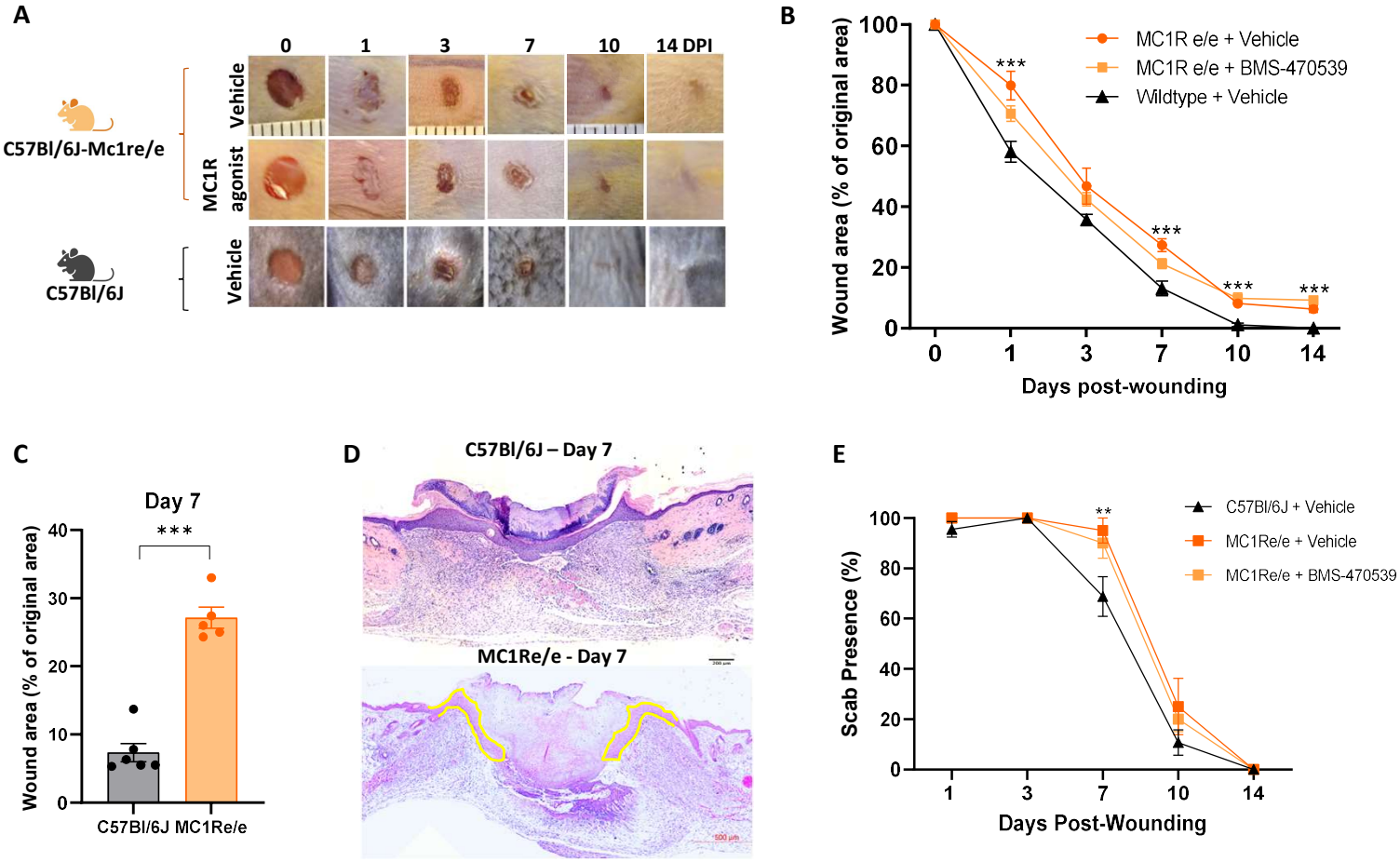

Figure 4 - Lack of functional MC1R impairs acute wound healing

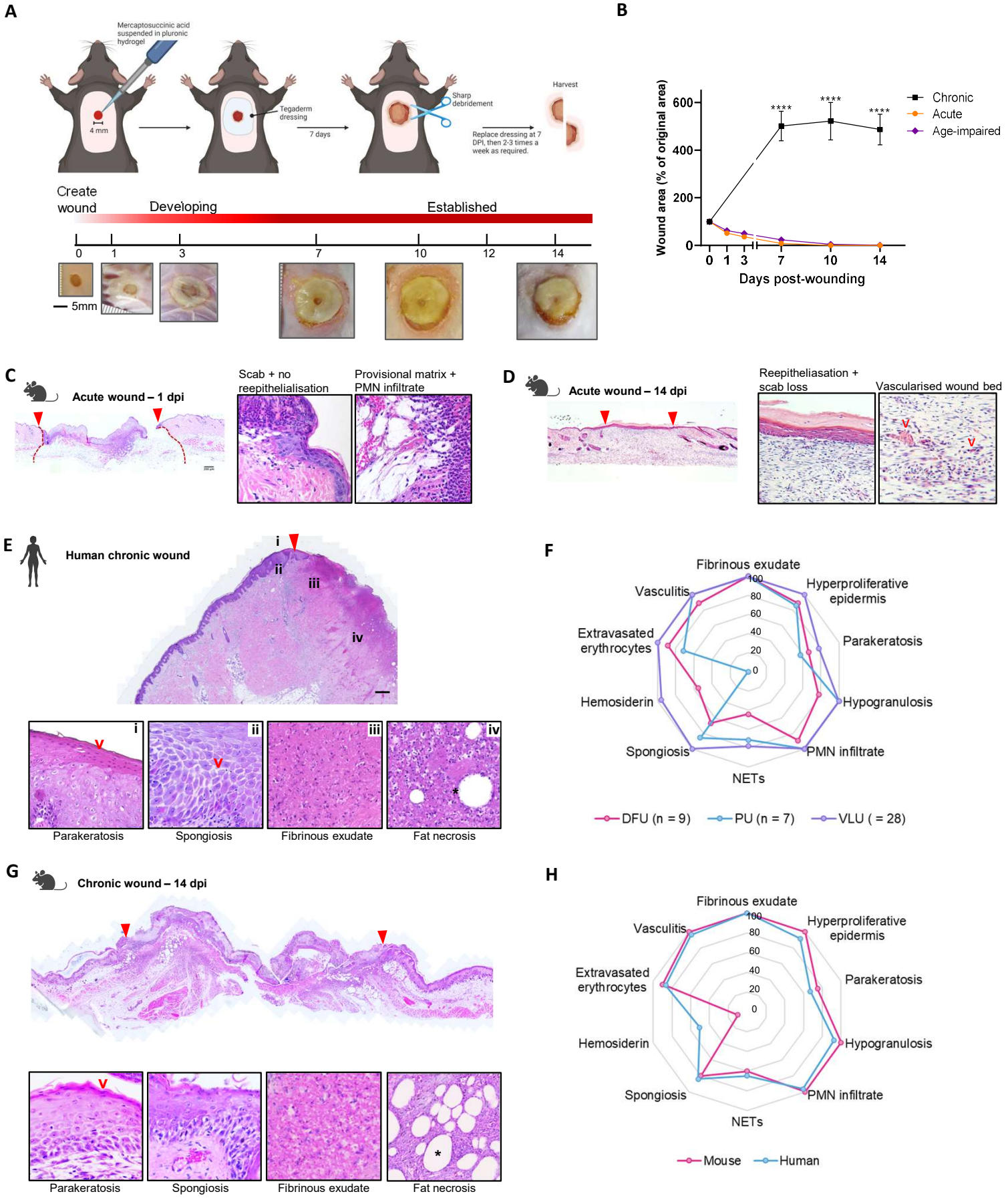

Figure 5 – Preclinical model recapitulates hallmarks of human chronic wounds

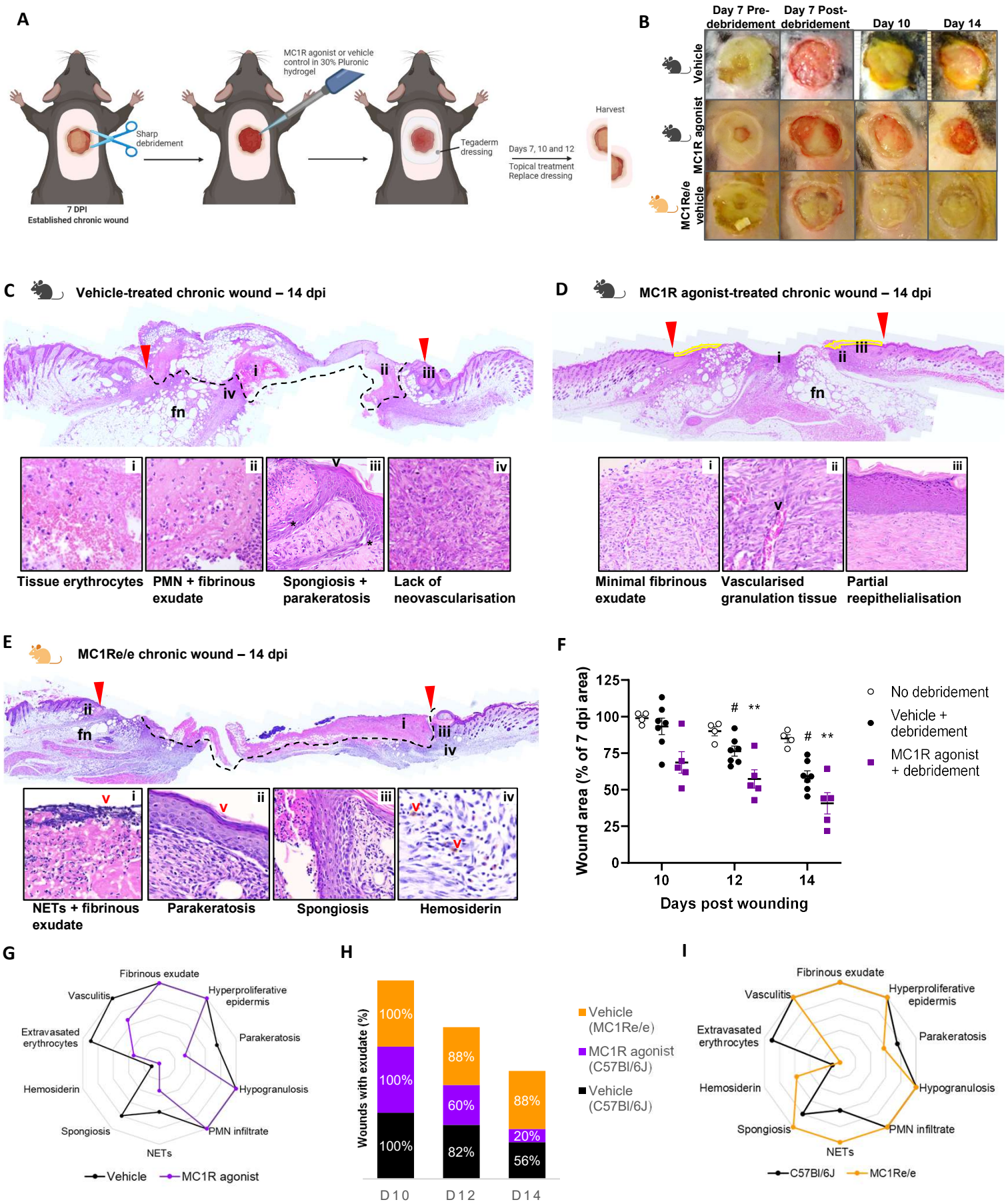

Figure 6 - MC1R agonist rescues the healing response in a preclinical chronic wound model

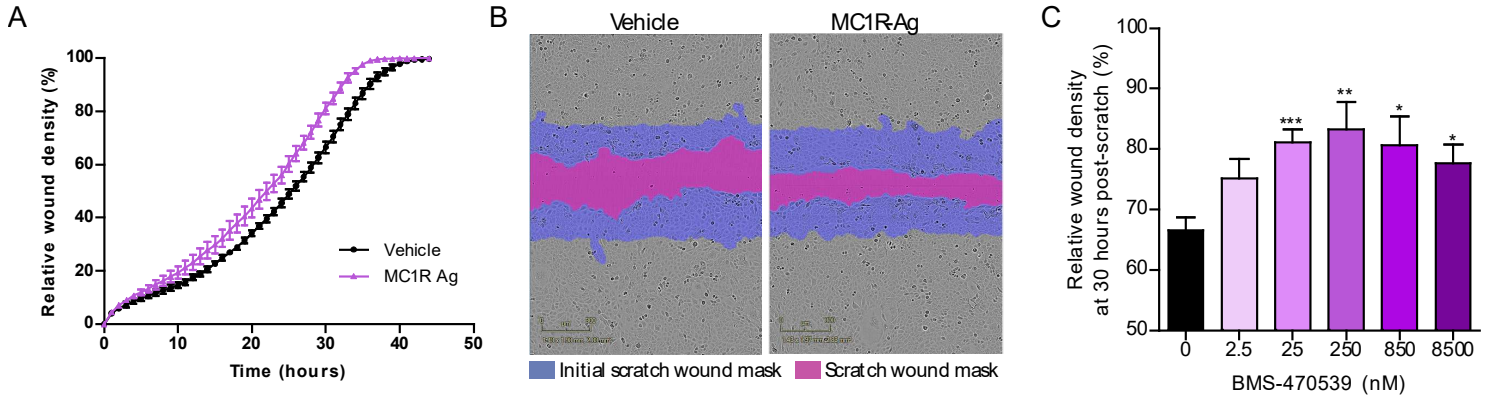

Figure S1 – MC1R agonist drives *in vitro* scratch wound closure

HaCaTs (human keratinocytes) were allowed to migrate for 15 hr to fill in a "scratch wound" *in vitro* in the presence of BMS-470539 or media control.

(A) Time course of scratch wound closure with vehicle or MC1R-Ag treatment (250 nM BMS-470539).

(B) Representative images taken at 7 h

(C) Dose response of scratch wound closure.

Data are expressed as mean ± SEM. * $p<0.05$, ** $p<0.01$, *** $p<0.001$ by two-way ANOVA with Bonferroni's multiple comparison test (A,C) relative to vehicle-treated wounds.

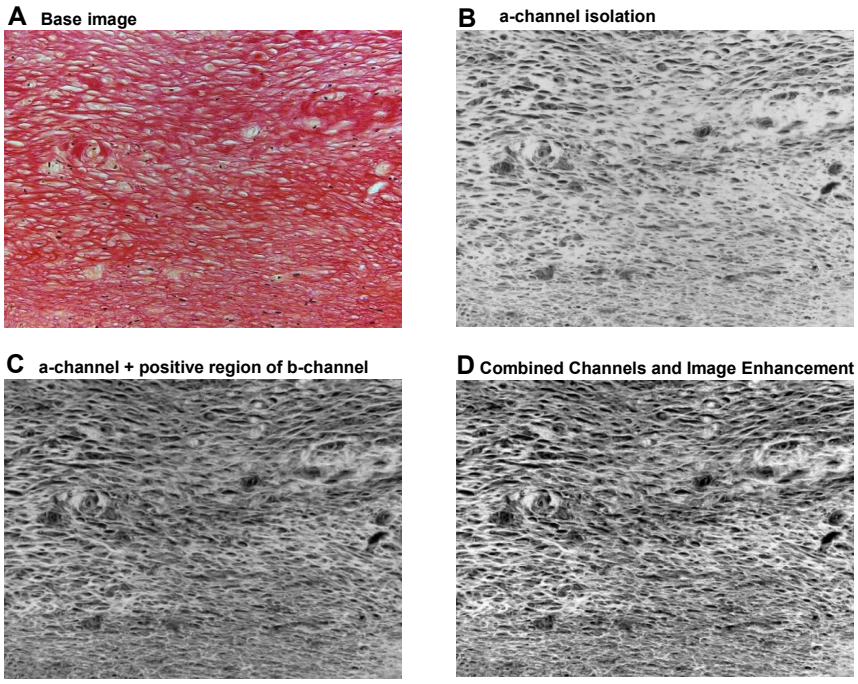

Figure S2 Progression of image preparation algorithm showing improved fibre clarity
(A) base image of picrosirius red-stained skin section.
(B) a-channel isolation after L*a*b conversion.
(C) combination of a-channel with positive region of b-channel.
(D) combined channels with contrast and brightness adjustment

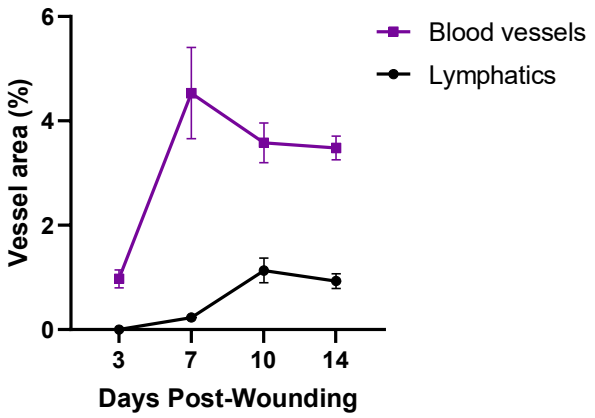

Figure S3 – Time course of wound angiogenesis and lymphangiogenesis
Quantification of CD31⁺ (blood vessel) area and Lyve-1⁺ (lymphatic vessel) area per hpf. Data are expressed as mean ± SEM. n=6 biological replicates and three independent experiments

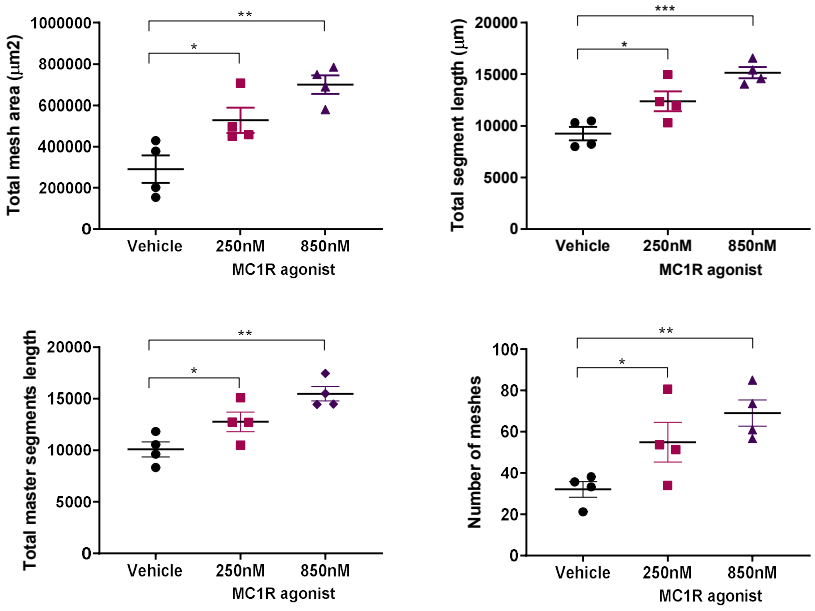

Figure S4 – MC1R agonist BMS-470539 promotes angiogenesis *in vitro*
Quantification of four key *in vitro* angiogenesis parameters in the presence and absence of MC1R agonist (250 nM and 850 nM). Data are expressed as mean ± SEM. Three independent experiments, each with five technical replicates.

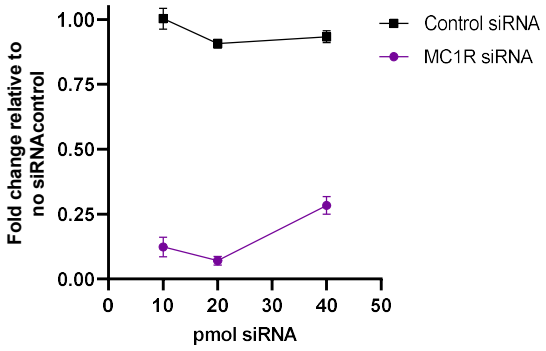

Figure S5 – MC1R siRNA knockdown vs control siRNA
Optimisation of MC1R siRNA knockdown. A dose of 20 pM was chosen. Data are expressed as mean ± SEM from three independent experiments, each with three technical replicates.

A

Ethical approval number

Animal number

dpi	Date	Wound		Wound Area				Activity and Movement	Behaviour			Irritation	Weight	Weight (%)	Pain	Bepanthen applied	Hair regrowth	Dressing		Photo Taken	Mash	Notes	Monitor (initials)	NVS spoken to	20% weight threshold	10% weight threshold
		Score	Exudate	Score	Size	Appearance		Score	Score	Scratching	Shaking							Appearance	Changes							
						Dead white tissue	Red ring around tissue																			
BASELINE	10.3.22												36								Yes				28.8	32.4
1	11.3.22	1	No Exudate	1	Growing larger	Yes	No	0	0	No	No	No	35.8	99.44%	0	No	No	Adherent	No		Yes					
2	12.3.22	1	Clear Exudate	1	No Change	Yes	Yes	0	0	No	No	No	34.2	95.00%	0	No	No	Adherent	No		Yes					
3	13.3.22	1	Clear Exudate	1	No Change	Yes	Yes	0	0	No	No	No	35.6	98.89%	0	No	No	Adherent	No		Yes	bit of crustiness next to dressing (leaked wound exudate)				
4	14.3.22	1	Clear Exudate	1	No Change	Yes	Yes	0	0	No	No	No	36.5	101.39%	0	No	No	Adherent	No		Yes	bit of crustiness next to dressing (leaked wound exudate)				
5	15.3.22	1	Clear Exudate	1	No Change	Yes	Yes	0	0	Yes	No	No	36.2	100.56%	0	No	No	Adherent	No		Yes	bit of crustiness next to dressing (leaked wound exudate)				
6	16.3.22	1	Clear Exudate	1	No Change	Yes	No	0	0	No	No	No	34.2	95.00%	0	No	No	Edges lifted	No		Yes					
7	17.3.22	1	Clear Exudate	1	No Change	Yes	No	0	0	No	No	No	34.2	95.00%	0	No	No	Adherent	Yes		Yes	Debrided, dressing change + PL treatment				
8	18.3.22	1	Clear Exudate	1	No Change			0	0	No	No	No	34.8	96.67%	0	No	No	Adherent	No		Yes					
9	19.3.22	1	Clear Exudate	1	No Change			0	0	Yes	No	No	34.3	95.28%	0	No	No	Adherent			Yes	bit of crustiness next to dressing (leaked wound exudate)				
10	20.3.22	1	Clear Exudate	1	No Change			0	0	No	No	No	34.2	95.00%	0	No	No	Adherent	Yes		Yes	Dressing change and PL treatment.				
11	21.3.22	1	Clear Exudate	1	No Change			0	0	No	No	No	33.7	93.61%	0	No	No	Adherent	No		Yes					
12	22.3.22	1	Clear Exudate	1	No Change			0	0	No	No	No	33.6	93.33%	0	No	No	Edges lifted	Yes		Yes	Large, sloughy, wet wound. Crusty. PL and dressing change.				
13	23.3.22	1	Clear Exudate	1	No Change			0	0	No	No	No	33.9	94.17%	0	No	No	Adherent	No		Yes	bit of crustiness next to dressing (leaked wound exudate)				
14	24.3.22	1	Clear Exudate	1	No Change			0	0	No	No	No	34	94.44%	0	No	No	Adherent	No		Yes					

B

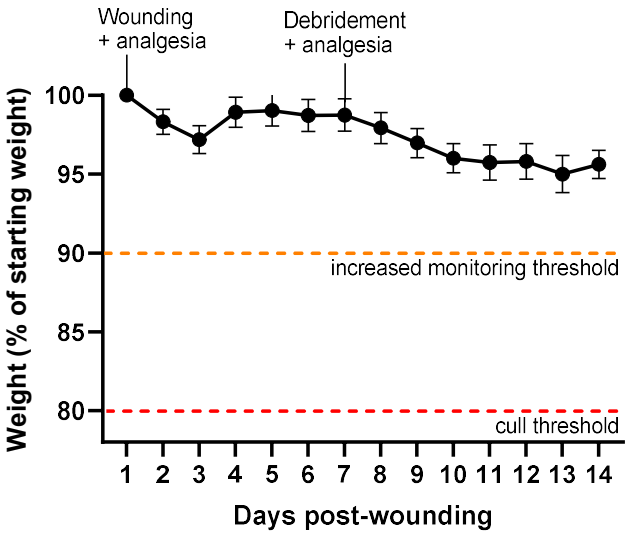

C

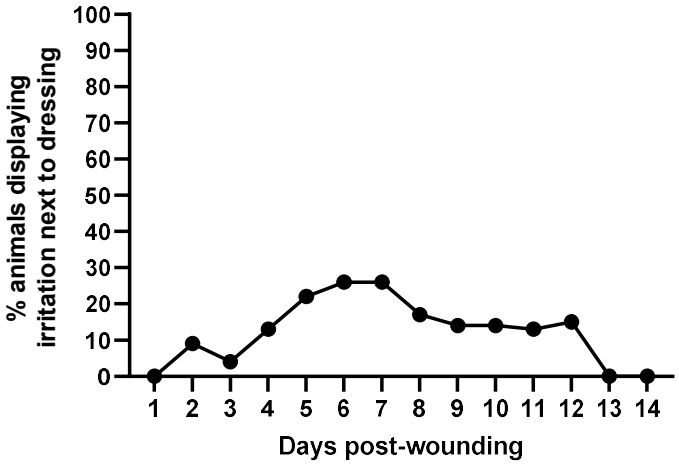

Figure S6 – Murine chronic wounds are very well tolerated

(A) Example monitoring record of wound features, animal behaviour and weight to ensure humane and ethical treatment.

(B) Minimal weight loss indicates that the chronic wound protocol is well tolerated by the aged mice. Data displayed as mean ± SEM (n=24).

(C) Up to 30% of mice displayed minor skin irritation next to the Tegaderm dressing. When this was observed Bepanthen cream was applied to soothe the area and prevent the irritation from worsening (n=24).

	DFU (n = 9)	PU (n = 7)	VLU (n = 28)	mean
Fibrinous exudate	100%	100%	100%	100%
Hyperproliferative epidermis	89%	86%	100%	92%
Parakeratosis	67%	57%	78%	67%
Hypogranulosis	78%	100%	100%	93%
PMN infiltrate	89%	100%	100%	96%
NETs	44%	71%	78%	65%
Spongiosis	67%	86%	100%	84%
Hemosiderin	56%	0%	96%	51%
Extravasated erythrocytes	89%	71%	100%	87%
Vasculitis	89%	100%	100%	96%

Figure S7 – Prevalence of key histomorphological features of human chronic wounds according to wound category

	Mouse	Human
Fibrinous exudate	100%	100%
Hyperproliferative epidermis	100%	92%
Parakeratosis	75%	67%
Hypogranulosis	100%	93%
PMN infiltrate	100%	96%
NETs	60%	65%
Spongiosis	80%	84%
Hemosiderin	10%	51%
Extravasated erythrocytes	90%	87%
Vasculitis	100%	96%

Figure S8 – Comparison of the prevalence of key features of human chronic wounds in mouse and human

Key features were scored by two independent assessors for 10 preclinical mouse wounds and 44 human chronic wounds (average of DFU, VLU and PU in Fig. S7).

	Vehicle	MC1R agonist
Fibrinous exudate	100%	100%
Hyperproliferative epidermis	100%	100%
Parakeratosis	75%	33%
Hypogranulosis	100%	100%
PMN infiltrate	100%	100%
NETs	60%	33%
Spongiosis	80%	0%
Hemosiderin	10%	0%
Extravasated erythrocytes	90%	33%
Vasculitis	100%	67%
Fat necrosis	100%	100%

Figure S9 – Prevalence of key histomorphological features of human chronic wounds in vehicle-treated and MC1R agonist-treated murine chronic wounds

	C57Bl/6J	MC1Re/e
Fibrinous exudate	100%	100%
Hyperproliferative epidermis	100%	100%
Parakeratosis	75%	57%
Hypogranulosis	100%	100%
PMN infiltrate	100%	100%
NETs	60%	100%
Spongiosis	80%	100%
Hemosiderin	10%	57%
Extravasated erythrocytes	90%	0%
Vasculitis	100%	100%
Fat necrosis	100%	100%

Figure S10 – Prevalence of key histomorphological features of human chronic wounds in wildtype C57Bl/6J and MC1Re/e murine chronic wounds

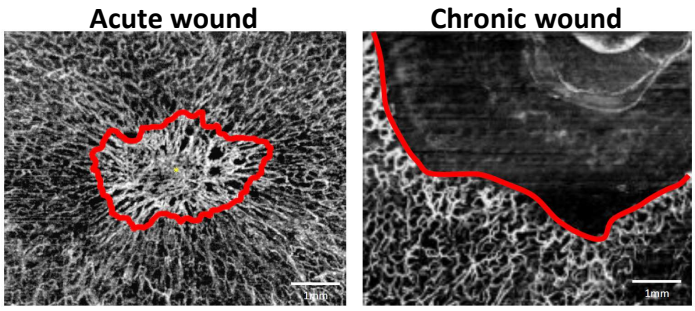

Figure S11 – OCT imaging of acute (A) and chronic (B) wounds at 7 dpi

(A) OCT enables visualisation of the perfused vasculature, demonstrating the increased vessel density in acute wounds during repair in comparison to the surrounding tissue (n=6).

(B) Human chronic wounds exhibit poor angiogenesis. Our preclinical wound model replicates this feature, displaying an almost complete lack of wound bed perfusion (n=2).

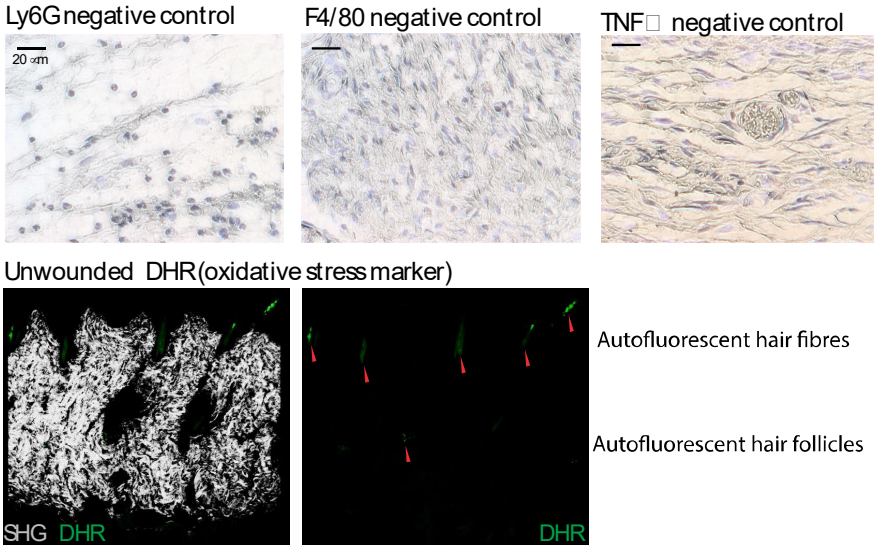

Figure S12
(A) Negative controls for immunohistochemical staining for Ly6G (neutrophils), F4/80 (macrophages) and TNFα.
(B) Negative controls for immunofluorescence staining of skin wound sections showing autofluorescent hair fibres and follicles.